PCCP

PAPER

A theoretical evaluation of possible transition metal electro-catalysts for N₂ reduction†

Egill Skúlason,[ab] **Thomas Bligaard,**[abc] **Sigríður Gudmundsdóttir,**[a] **Felix Studt,**[c] **Jan Rossmeisl,**[b] **Frank Abild-Pedersen,**[c] **Tejs Vegge,**[d] **Hannes Jónsson**[ac] **and Jens K. Nørskov**[*ce]

Theoretical studies of the possibility of forming ammonia electrochemically at ambient temperature and pressure are presented. Density functional theory calculations were used in combination with the computational standard hydrogen electrode to calculate the free energy profile for the reduction of N₂ admolecules and N adatoms on several close-packed and stepped transition metal surfaces in contact with an acidic electrolyte. Trends in the catalytic activity were calculated for a range of transition metal surfaces and applied potentials under the assumption that the activation energy barrier scales with the free energy difference in each elementary step. The most active surfaces, on top of the volcano diagrams, are Mo, Fe, Rh, and Ru, but hydrogen gas formation will be a competing reaction reducing the faradaic efficiency for ammonia production. Since the early transition metal surfaces such as Sc, Y, Ti, and Zr bind N-adatoms more strongly than H-adatoms, a significant production of ammonia compared with hydrogen gas can be expected on those metal electrodes when a bias of − 1 V to − 1.5 V *vs.* SHE is applied. Defect-free surfaces of the early transition metals are catalytically more active than their stepped counterparts.

1 Introduction

Ammonia is among the chemicals produced in the largest quantities in the chemical industry, where it is primarily used in the production of fertilizers. For more than a hundred years, ammonia has been produced by the Haber–Bosch process, a discovery that has been of key importance in supporting the large global population growth over the past century.[1] Much work has gone into the optimization of this process and today it is understood in great detail.[2–10] In the Haber–Bosch process, nitrogen and hydrogen gas molecules are heated to approximately 400 °C, pressurized to around 150 bar and passed over an Fe-based catalyst to form ammonia:[6,8]

$$N_2 + 3H_2 \rightarrow 2NH_3 \qquad (1)$$
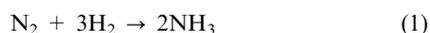
Although the reaction is exothermic, relatively high temperature is required to make the reaction kinetics fast. This, however, shifts the equilibrium towards the reactants resulting in lower conversion. The high pressure is chosen to alleviate this problem, since it shifts the equilibrium in favor of the products.

The industrial conditions are in remarkable contrast to those in microorganisms which exist in nature and use the enzyme nitrogenase to produce ammonia from solvated protons, electrons and atmospheric nitrogen under ambient conditions. The active site in the enzyme is a MoFe₇S₉N cluster, the FeMo-cofactor, which catalyzes the electrochemical reaction:

$$N_2 + 8H^+ + 8e^- \rightarrow 2NH_3 + H_2 \qquad (2)$$

While the reaction has $\Delta G \simeq 0$ at pH = 7 and standard conditions, at least 16 adenosine triphosphate (ATP) molecules (or approximately 5 eV)[11,12] are used to facilitate the reaction. Nitrogenase can thus be viewed as part of an ATP driven electrochemical cell for this reaction. It is conceivable that this process could be emulated in a simpler, man-made system.[13,14] A low-temperature, low-pressure process could make more decentralized ammonia production possible compared with the current situations where ammonia can only be produced in large factories. The protons could come from water splitting, while the electrons would be driven to the electrode surface by

a Science Institute and Faculty of Science, VR-III, University of Iceland, IS-107 Reykjavik, Iceland
b Center for Atomic-scale Materials Design, Department of Physics, Technical University of Denmark, Building 311, DK-2800 Kgs. Lyngby, Denmark
c SUNCAT Center for Interface Science and Catalysis, SLAC National Accelerator Laboratory, 2575 Sand Hill Road, Menlo Park, CA 94025, USA
d Materials Research Division, Risø National Laboratory for Sustainable Energy, Technical University of Denmark, DK-4000 Roskilde, Denmark
e Department of Chemical Engineering, Stanford University, Stanford, CA 94305, USA. E-mail: norskov@stanford.edu

This journal is © the Owner Societies 2012

Phys. Chem. Chem. Phys., 2012, **14**, 1235–1245 | 1235

an applied bias. The reaction mechanism in enzymes is quite different from that of the industrial synthesis process. In the enzyme, N_2 molecules are hydrogenated (*associative mechanism*),[15–18] while in the Haber–Bosch method, the nitrogen and hydrogen atoms do not react until the strong N_2 triple bond and the H_2 bond have been broken (*dissociative mechanism*).[13]

It has been shown that transition metal complexes based on molybdenum can reduce N_2 to ammonia for the artificial process at room temperature and ambient pressure.[19] The energy input needed for artificial processes is estimated to be as large as for the biological N_2 fixation.[20] For the electrocatalytic N_2 reduction, various types of electrolytes and electrode materials have been tried, but the kinetics are too slow for practical applications.[21–28] Little is known about the mechanism of this process and in most cases hydrogen gas is formed more readily than hydrogenation of N_2.

In the present study, reactions on Ru surfaces were first studied, since this is the optimal pure metal catalyst for the industrial process.[29] Density functional theory (DFT) calculations of ammonia formation on both the flat and stepped surface were carried out. For each surface, the reduction of both the adsorbed N_2 molecule and adsorbed N atoms were studied. The influence of an external potential was subsequently taken into account using the computational standard hydrogen electrode[30] and the lowest overpotential required to reduce nitrogen into ammonia was estimated. The free energy of the various intermediates formed on the surfaces was calculated as a function of voltage. The binding energies of the adsorbed species on a range of close-packed and stepped transition metal surfaces were calculated and used to identify the most active transition metal catalyst in forming ammonia instead of hydrogen.

2 Methodology

2.1 DFT calculations

A close-packed hcp(0001) surface was used to model the flat surfaces of Sc, Y, Ti, Zr Re, Os, Co, and Ru while a fcc(111) surface was used for Rh, Ir, Ni, Pd, Pt, Cu, Ag, and Au and a bcc(110) surface was used for V, Nb, Ta, Cr, Mo, W, and Fe. The calculations were carried out using DFT with the RPBE functional[31,32] implemented in the Dacapo code. Plane wave basis sets were used to simulate a periodically repeated (2×2) three layer supercell. The stepped surfaces were modeled with (6×2) three layer cells, where three rows of the metal atoms in the top layer were removed to create a strip island three rows wide. Increasing the strip size to five rows was found to change the adsorption energy in test cases by less than 0.1 eV. The calculated lattice constants were: Sc 3.30 Å (*c*/*a* ratio: 1.59), Ti 2.96 Å (*c*/*a* ratio: 1.59), Re 2.76 Å (*c*/*a* ratio: 1.62), Os 2.76 Å (*c*/*a* ratio: 1.58), Co 2.48 Å (*c*/*a* ratio: 1.62), Ru 2.75 Å (*c*/*a* ratio: 1.58), Y 3.68 Å (*c*/*a* ratio: 1.57), Zr 3.26 Å (*c*/*a* ratio: 1.59), Rh 3.85 Å, Ni 3.56 Å, Ir 3.87 Å, Pt 4.02 Å, Pd 4.02 Å, Cu 3.71 Å, Ag 4.21 Å, Au 4.22 Å, Ta 3.33 Å, V 3.02 Å, Nb 3.33 Å, W 3.20 Å, Mo 3.20 Å, Cr 2.87 Å, and Fe 2.91 Å. The slabs were separated by 10–12 Å of vacuum. For the close-packed surfaces, the two bottom metal layers were fixed and

the top layer was allowed to relax as were the adsorbed species. For the stepped surfaces, the two top close-packed layers were allowed to relax, whereas the bottom layer was fixed. The structural optimizations were considered converged when maximum force in any direction on any moveable atom was less than 0.01 eV Å^{-1}.

All the DFT calculations were spin restricted except those for Ni, Fe, and Co, where spin-polarized calculations were made. The self-consistent electron density is determined by iterative diagonalization of the Kohn–Sham Hamiltonian, with the occupation of the Kohn–Sham states being smeared according to a Fermi–Dirac distribution with a smearing parameter of $k_B T = 0.1$ eV. All calculated values of the energy have been extrapolated to $k_B T = 0$ eV. A $6 \times 6 \times 1$ Monkhorst–Pack k-point sampling was used for the flat Ru surfaces and maximum symmetry was applied to reduce the number of k-points in the calculations. For all the other metals, a $4 \times 4 \times 1$ k-point sampling was used since the difference between this and the denser k-point sampling was found to be less than 0.01 eV in test calculations. A $2 \times 6 \times 1$ k-point sampling was used for all the stepped surfaces. The plane wave cutoff was 30 Ry for the wave function and 60 Ry for the density for the Ru calculations, whereas these values were 25 Ry and 36.7 Ry, respectively, for all the other metals.

2.2 Electrochemical reactions

As a convenient reference we take the source of protons and electrons to be the anode reaction

$$H_2 \rightleftharpoons 2H^+ + 2e^- \qquad (3)$$

The protons are solvated in the electrolyte and the electrons are transported from the anode to the cathode through a wire. At the cathode the reaction is

$$N_2 + 6H^+ + 6e^- \rightarrow 2NH_3, \qquad (4)$$
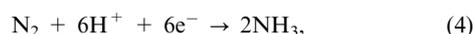
where nitrogen molecules, protons and electrons react to form ammonia. The overall electrochemical reaction is, therefore, reaction (1).

In principle, four different types of reaction mechanism are possible for the electrochemical ammonia synthesis. Associative or dissociative pathways where either adsorbed N_2H_x or NH_x species can be hydrogenated are possible. In addition, both these pathways could include a Tafel-type mechanism[33] where the solvated protons from the solution first adsorb on the surface and combine with electrons and then the hydrogen adatoms react with adsorbed N_2H_x or NH_x species. The other possible reaction mechanism is a Heyrovsky-type reaction[34] where the adsorbed N_2H_x or NH_x species are hydrogenated by direct attachment of protons from the solution and electrons from the electrode. In the latter case an applied bias can directly affect the thermochemical barrier, whereas in the Tafel-type reaction it can only have an indirect effect through varying the concentrations of the reactants.[35,36] In this study we are considering a room temperature process and since the activation barriers for the Tafel-type $*H + *NH_x \rightarrow *NH_{x+1}$ reactions are about 1 eV or higher for most transition metal surfaces[10,37] a Tafel-type mechanism will be very slow. The process will therefore either go through an associative or

dissociative Heyrovsky-type reaction. Similar assumptions have been made in the electrochemical reduction of O_2 and CO_2.[30,38,39]

First, we consider the possibility that the reaction follows an *associative Heyrovsky mechanism*, where the nitrogen molecules are hydrogenated by protons, analogous to the mechanism in the enzyme (an asterisk, *, denotes a site on the surface):

$$* + N_2 \rightarrow {}^*N_2 \qquad (5)$$

$${}^*N_2 + 6(H^+ + e^-) \rightarrow {}^*N_2H + 5(H^+ + e^-) \qquad (6)$$

$${}^*N_2H + 5(H^+ + e^-) \rightarrow {}^*NNH_2 + 4(H^+ + e^-) \qquad (7a)$$

$${}^*N_2H + 5(H^+ + e^-) \rightarrow {}^*NHNH + 4(H^+ + e^-) \qquad (7b)$$

$${}^*NNH_2 + 4(H^+ + e^-) \rightarrow {}^*N + NH_3 + 3(H^+ + e^-) \qquad (8a)$$

$${}^*N_2H_2 + 4(H^+ + e^-) \rightarrow {}^*NHNH_2 + 3(H^+ + e^-) \qquad (8b)$$

$${}^*N + 3(H^+ + e^-) \rightarrow {}^*NH + 2(H^+ + e^-) \qquad (9)$$

$${}^*NH + 2(H^+ + e^-) \rightarrow {}^*NH_2 + (H^+ + e^-) \qquad (10)$$

$${}^*NH_2 + (H^+ + e^-) \rightarrow {}^*NH_3 \qquad (11)$$

$${}^*NH_3 \rightarrow NH_3 + * \qquad (12)$$
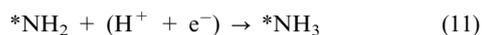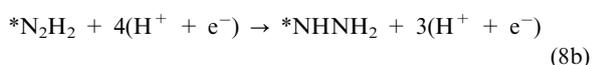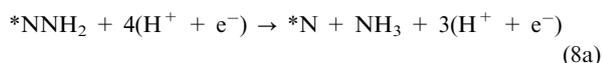
where ${}^*N_2H_2$ in (8b) can be either ${}^*NNH_2$ or ${}^*NHNH$. Since reaction (8a) is much more favorable than (8b) we continue with ${}^*N$ on the surface in eqn (9). Then, we consider a *dissociative Heyrovsky mechanism*, where the nitrogen molecules are first dissociated on the surface and subsequently hydrogenated by direct attachment of protons from the solution:

$$2* + N_2 \rightarrow 2{}^*N \qquad (13)$$

$$2{}^*N + 6(H^+ + e^-) \rightarrow {}^*N + {}^*NH + 5(H^+ + e^-) \qquad (14)$$

$${}^*N + {}^*NH + 5(H^+ + e^-) \rightarrow 2{}^*NH + 4(H^+ + e^-) \qquad (15)$$

$$2{}^*NH + 4(H^+ + e^-) \rightarrow {}^*NH + {}^*NH_2 + 3(H^+ + e^-) \qquad (16)$$

$${}^*NH + {}^*NH_2 + 3(H^+ + e^-) \rightarrow 2{}^*NH_2 + 2(H^+ + e^-) \qquad (17)$$

$$2{}^*NH_2 + 2(H^+ + e^-) \rightarrow {}^*NH_2 + {}^*NH_3 + (H^+ + e^-) \qquad (18)$$

$${}^*NH_2 + {}^*NH_3 + (H^+ + e^-) \rightarrow 2{}^*NH_3 \qquad (19)$$

$$2{}^*NH_3 \rightarrow {}^*NH_3 + NH_3 + * \qquad (20)$$

$${}^*NH_3 + NH_3 \rightarrow 2NH_3 + 2* \qquad (21)$$
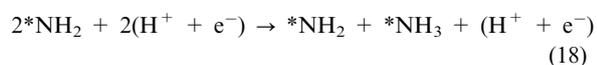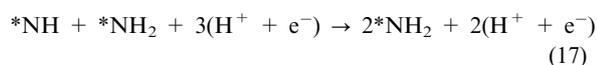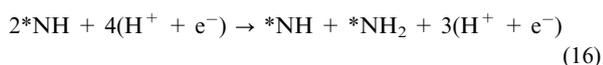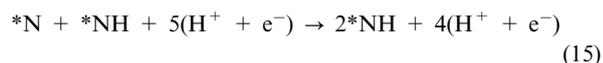
DFT calculations were used to estimate the free energy of each elementary step. The calculations provide information about the stability of various possible surface intermediates, which is difficult to obtain by other means. The adsorption energy and vibrational frequencies for the most stable configuration of each intermediate were calculated and the free energy could thus be estimated within a harmonic approximation as a function of applied potential. On this basis, we establish a

reaction mechanism and estimate the thermochemistry of the cathode reactions. The computational standard hydrogen electrode was introduced in ref. 30 for describing trends in electrochemical oxygen reduction. Here, we apply it to the reduction of N and N_2 in an electrochemical cell. The procedure involves 5 steps:

(1) The reference potential is set to be that of the standard hydrogen electrode (SHE). The chemical potential (the free energy per H) of $(H^+ + e^-)$ is related to that of $\frac{1}{2}H_2$ (eqn (3) is in equilibrium). This means that at pH = 0, the potential of $U = 0$ V relative to the SHE and 1 bar of H_2 in the gas phase at 298 K, the reaction free energy of reaction (1) is equal to that of the net reaction of (5)–(12) or (13)–(21) at an electrode.

(2) The free energy of the intermediates is calculated at zero potential and pH = 0

$$\Delta G = \Delta E + \Delta E_{ZPE} - T\Delta S, \qquad (22)$$

where ΔE is the reaction energy. ΔE_{ZPE} and ΔS are the differences in zero point energy and entropy, respectively, between the adsorbed species and the gas phase molecules. The vibrational frequencies of the adsorbed species are calculated using normal mode analysis with DFT calculations and they are used to determine the zero point energy correction and vibrational entropy of the adsorbed species, as described in ref. 36. The gas phase values are taken from standard molecular tables.[40]

(3) The effect of an applied bias, U, is included for all electrode reactions involving an electron by shifting the free energy by $-neU$, where n is the number of electrons involved in the reaction

$$\Delta G(U) = \Delta E + \Delta E_{ZPE} - T\Delta S - neU. \qquad (23)$$

(4) The effect of the electric field at the surface is taken into account. The simplest estimate involves introducing an external sawtooth potential with a potential drop in the vacuum, hence creating an electric field at the surface.[30,41–43] This field interacts with the dipole moment of the adsorbed species. Earlier estimates of the effect on the free energy have found the effect to be small. For example, the adsorption energy of O* and HO* has been estimated to change by less than 0.015 eV at $+1$ V bias where the Helmholtz layer was assumed to be 3 Å thick.[30] The field effect on the adsorption energy of the N_2, N, NH_2 and NNH species adsorbed on steps and on flat surfaces is from -0.02 to $+0.05$ eV when changing the bias by -0.9 V ($+0.3$ V Å^{-1} field) and from -0.06 to $+0.13$ eV when applying a -2.7 V bias ($+0.9$ V Å^{-1}). The field effects on the ZPE are even smaller than on the potential energy, or <0.01 eV and 0.01 eV when applying $+0.3$ V Å^{-1} and $+0.9$ V Å^{-1} electric field, respectively. These effects are neglected since they are much smaller than typical error estimates associated with DFT/GGA calculations, and are not likely to change the trends studied here.

(5) It is known that the presence of water may help stabilize some species more than others *via* hydrogen bonding. For example *NH is expected to be stabilized by hydrogen bonding, while the effect of the water layer on adsorbed nitrogen will be negligible. The effect of hydrogen-bonded stabilization of the adsorbates has been included in the following approximative way.

This journal is © the Owner Societies 2012

Phys. Chem. Chem. Phys., 2012, **14**, 1235–1245 | 1237

We include hydrogen bonds using information for hydrogen bonds of *O–H (0.5 eV)[30,44,45] and *O–O–H (0.25 eV)[46] adsorbed on a surface. This is 0.25 eV per H-bond of the OH⋯:O type. We then divide these numbers by 3, according to the difference in strength of the H-bonds of the OH⋯:O type vs. NH⋯:O type in gas phase.[47] Similar assumptions have been made previously for the intermediates in the CO_2 reduction.[39]

Explicit inclusion of water in the simulations would increase the computational effort tremendously and has not been included in this study, since here we are trying to get a qualitative picture of where to search for a catalyst for the N_2 reduction into ammonia. The preferred adsorption geometry can change dramatically by the explicit inclusion of water, in particular in methanol adsorption on Pt(111).[48] There, the effect was large because the OH group binds to the surface in the absence of water, but gets pointed away from the surface to form hydrogen bonds in the presence of water. In the cases presented here, the protons that can form hydrogen bonds with water molecules are already pointing away from the surface so a significant change in the geometry is not expected.

In the present reaction, *OH and *O species could poison the surface sites; especially the stepped surfaces and all surface sites of the early transition metals. However, at a sufficiently negative bias needed for the N_2 reduction, the *OH and *O species are reduced to water.

At pH-values different from 0, the free energy of H^+-ions should be corrected for the concentration dependence of the entropy, $G(pH) = -kT \times \ln[H^+] = kT \times pH \times \ln 10$. All calculations presented here are for pH = 0.

2.3 Estimating trends in reactivity

The adsorption energies of all intermediate states in (5)–(21) were calculated for the flat and stepped surfaces for a range of transition metals. The results were used to estimate the free energy change in the elementary reactions (5)–(12) and (13)–(21). The negative of the free energy difference of an elementary step, $-\Delta G$, is used as a simple measure of the onset potential (theoretical overpotential) needed for these reactions to have a reasonable rate.

Trends in catalytic activity of the transition metals can be summarized and interpolated using approximate linear relations for the adsorption energy.[49] It has been shown that the adsorption energies of simple hydrogen containing species AH_x (for example, CH_x ($x = 1, 2, 3$), NH_x ($x = 1, 2$), OH_x ($x = 1$) and SH_x ($x = 1$)) depend nearly linearly on the adsorption energy of the atom A. Larger carbon containing molecules have been shown to scale with adsorption of C as well.[50] In this paper we establish linear relations for N_2H_x ($x = 0, 1, 2$) molecules using the chemisorption energy of the N-adatom as the descriptor. Within this approximate scheme, we construct so-called volcano plots where the onset potential and the most catalytically active metal surface can be identified.

3 Results

3.1 Ammonia formation on a flat and stepped Ru(0001) surface

We first present results of calculations of the reduction of nitrogen via the associative and dissociative mechanisms on
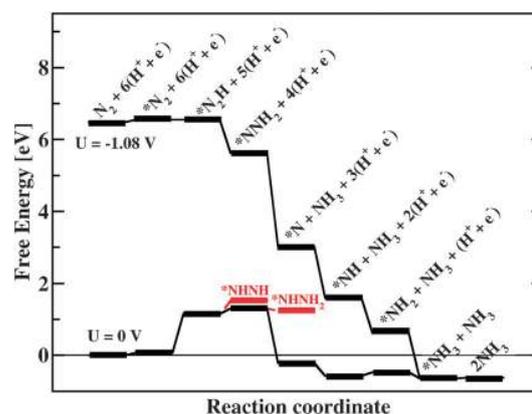
Fig. 1 Free energy for the associative mechanism on a flat Ru(0001) surface obtained from DFT calculations of the binding energy and vibrational frequencies, as well as entropy of the gas molecules. For an electrolyte with pH = 0 at 300 K, this also gives the free energy for the electrochemical reaction when there is no applied bias, $U = 0$ V. The most difficult step is the addition of the first proton to the adsorbed N_2 molecule. With an applied potential of $U = -1.08$ V, all the elementary steps involve either no change or a decrease in free energy.

the Ru(0001) surface. All intermediates are included and the free energy is referenced to N_2 and H_2 in the gas phase. Similar results have previously been published for the dissociative mechanism on flat and stepped Ru(0001) and the associative mechanism on flat Ru(0001),[13,51,52] but the results on the associative mechanism at a step are new. In the Discussion section, we use these results to predict the electrochemical analogs of each step of these different mechanisms.

Hydrogen atoms are added one by one to the adsorbed species and DFT calculations are used to find the minimum energy configuration, binding energy and vibrational frequencies. Several structures and adsorption sites were investigated in each case. In the Discussion section below, we add the influence of an applied electric potential. The DFT calculations show that an intact N_2 molecule binds on the flat Ru(0001) surface with an adsorption energy of -0.4 eV. The free energy change under ambient conditions is estimated to be $+0.08$ eV because of the large loss in entropy in going from the gas phase to a surface bound molecule, see Fig. 1. The most exergonic step, or the potential determining step, in the reduction to form ammonia is the addition of the first hydrogen atom to form N_2H. This first hydrogenation step is 0.75 eV uphill in energy and 1.08 eV in free energy (after including ZPE and entropy). A large entropy loss is also associated with the binding of hydrogen from the gas phase.

The intact N_2 binds more strongly at a step on the Ru(0001) surface, with an adsorption energy of -0.71 eV. This drop in energy is sufficiently large to make the free energy of adsorption -0.23 eV despite the significant loss in entropy from the gas phase, see Fig. 2. The addition of a hydrogen atom is again uphill in free energy and the addition of the second hydrogen atom even slightly more uphill in Fig. 2a whereas the first hydrogen step is most uphill in free energy in Fig. 2b.

The minimum energy configurations of the N_2H_x admolecules at the step are shown in Fig. 2c. A particularly stable configuration of the adsorbed N_2H molecule was found where
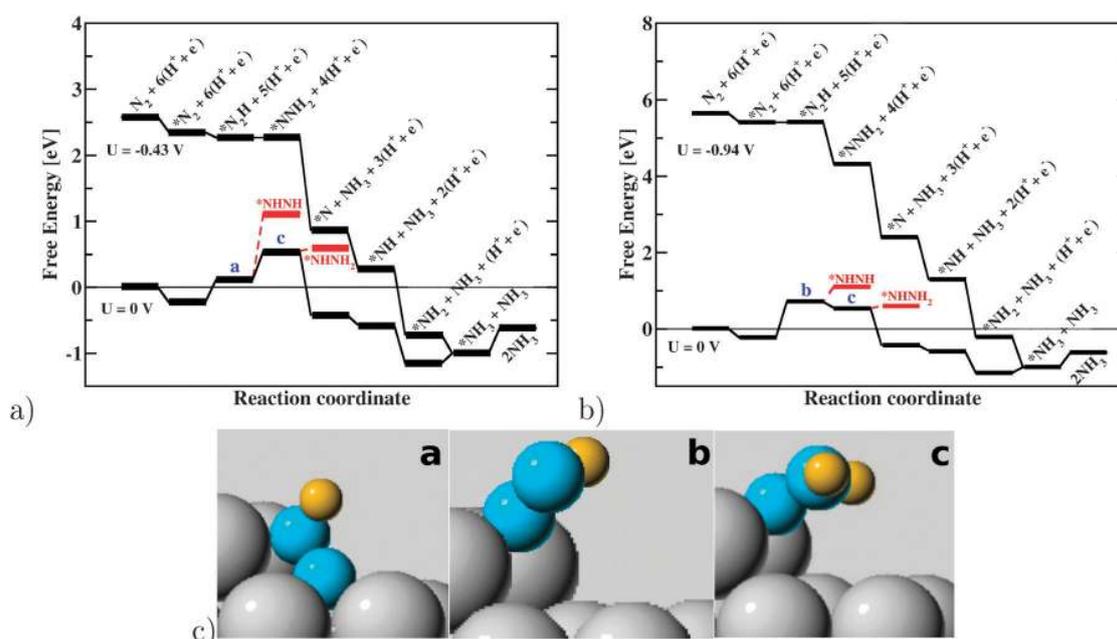
Fig. 2 Free energy for the associative mechanism at a step on the Ru(0001) surface, analogous to Fig. 1. The most difficult step is the addition of (a) the second proton or (b) the first proton to the N_2 molecule adsorbed at the step. With an applied potential of (a) $U = -0.43$ V or (b) $U = -0.94$ V, all the elementary steps involve either no change or a decrease in free energy. (c) Minimum energy configurations of N_2H and NNH_2. Configuration a shows N_2H adsorbed at the step and also bound to the terrace on the Ru(0001) surface. One N-atom is bound to the step at a bridge site with N–Ru bond lengths of 2.188 Å while the other N atom is bound to the terrace at a 3-fold hollow site with bond lengths of 2.09 Å on average. In configuration b the N_2H is adsorbed only at the step at a bridge position with N–Ru bond lengths of 2.058 Å. Configuration c shows NNH_2 adsorbed at a bridge position of a step with N–Ru bond lengths of 2.027 Å. A side view and top view of the various admolecules on the stepped Ru surface are shown in Fig. S1 in the ESI.† Color code: Ru, grey; N, blue; H, yellow.
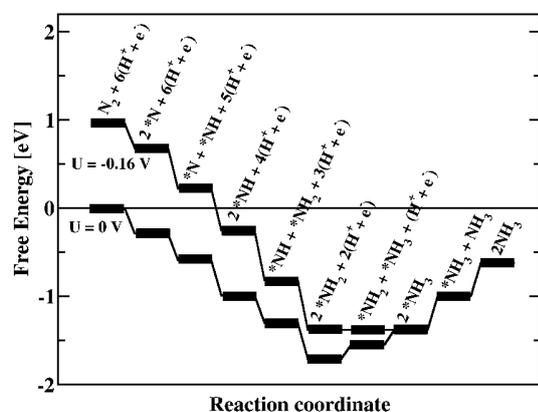
Fig. 3 Free energy for dissociative mechanism at a step on the Ru(0001) surface, analogous to Fig. 1 and 2. A predicted free energy profile for an applied potential of -0.16 V is also shown. This is the bias needed to prevent an increase in free energy at the potential determining step. The adsorbed ammonia molecules would then get further protonated to NH_4^+ and enter the solution (not shown).

the molecule bends down towards the surface so that both N atoms become bonded to metal atoms (configuration a). This significantly reduces the free energy barrier for the reduction as compared to the flat surface and makes the addition of the second hydrogen atom most uphill in free energy at the step. In Fig. 2b we have also included the possibility of reacting through the configuration labeled b since it does not involve a terrace site

under the step. Under realistic conditions, the surface is expected to be covered with hydrogen. Trends in both reaction mechanisms throughout the periodic table are discussed below.

It is well-established that dissociation of N_2 can only take place at steps on the Ru catalyst surface, because there is a prohibitively high energy barrier for dissociation on the flat terrace,[51] on the order of 1.9 eV. Fig. 3 shows the free energy diagram for the formation of ammonia at the stepped Ru(0001) surface *via* such a dissociative pathway at room temperature. In this case, the step most uphill in free energy would be the reduction of $*NH_2$ to $NH_{3(g)}$. Similar results were presented in ref. 52, but are included here for completeness.

3.2 Adsorption of H, N, NH_x and N_2H_x on other transition metals

To estimate the trends in catalytic activity of the transition metals in the associative reduction of nitrogen, a calculation of the binding of NH_x and N_2H_x ($x = 0, 1, 2$) molecules has been carried out on a range of metal surfaces, both the flat and the stepped surfaces. The metals span a wide range in binding energies. The binding energy of N_2H_x was found to scale quite well with the binding energy of N, analogous to what has been found for AH_x (A = C, N, O, and S) and C_2H_x type molecules previously.[49,50] Fig. 4a presents the same DFT calculations as in ref. 49 (of NH_x species) whereas here we have added more of the early transition metals: Y, Ti, Zr, Ta, V, Nb, Cr, W, Os, and Fe. The results for N_2H_x species on flat surfaces are shown
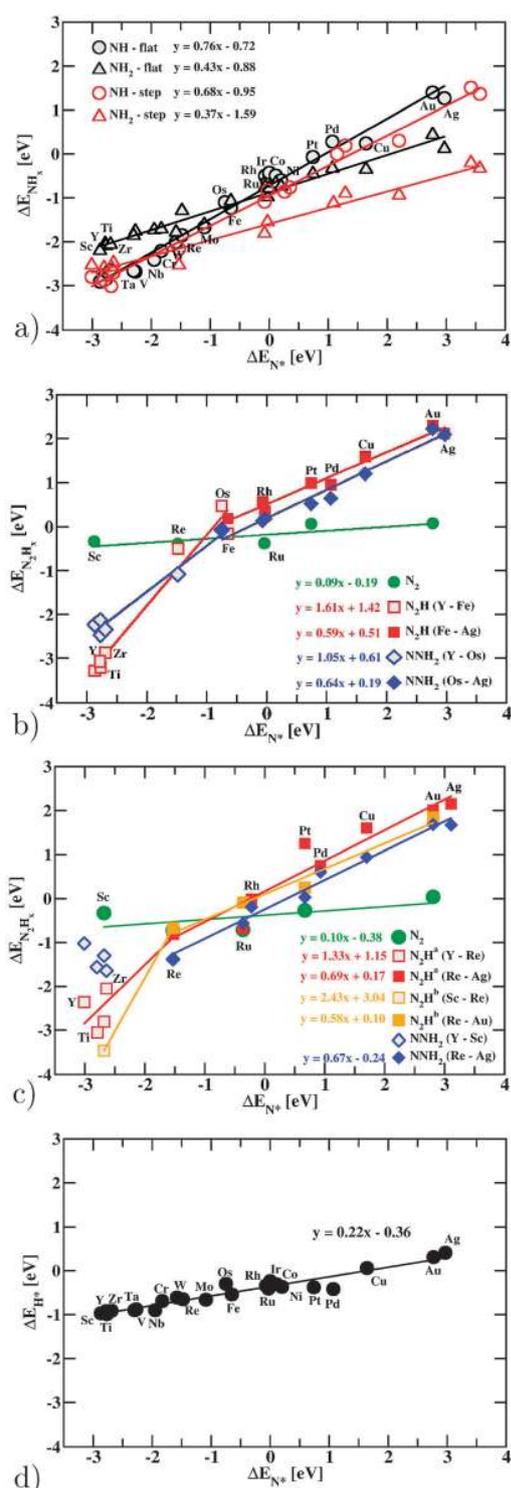
Fig. 4 Adsorption energy of (a) NH_x admolecules on both flat and stepped transition metals and in (b) and (c) the adsorption energy of N_2H_x admolecules as a function of the chemisorption energy of N on selected transition metals, both for (b) flat surfaces and (c) steps. (d) Adsorption energy of H adatoms as a function of the chemisorption energy of N adatoms on selected, close packed transition metal surfaces.

in Fig. 4b, where the N_2H_x energy is plotted against the adsorption energy of N. The linear relations of the N_2H_x

binding energy at a step are shown in Fig. 4c. The results are similar to those obtained for the flat surfaces. The slopes are similar, whereas the intercepts are slightly more negative for the steps since the steps tend to bind intermediates to the surface relatively stronger than the flat surfaces.

The closed shell molecule N_2 binds only weakly and with similar strength to all these transition metals, so its binding energy is largely independent of the binding energy of N. The adsorption energy of the N_2H_x radicals, however, scales in a different way for the early transition metals than for the late transition metals. In the former case, the slope is higher than one since both nitrogen atoms in the N_2H_x species form bonds to the surfaces and the bond between the N–N atoms has increased to 1.43 Å on average (cf. Tables I–IV in the ESI†). In the latter case, the N_2H_x species bind only with one of the N to the surface (except for the N_2H^a configuration on the steps) and the average bond length is shorter (1.30 Å). The slopes are all around 2/3 for both N_2H and N_2H_2 on both flat and stepped surfaces. The binding energy of the NNH_2 species on Y, Ti, Sc and Zr does not fall on the line because of large surface relaxation effects. This does not affect any of the remaining results since on those surfaces N_2 will dissociate immediately.

In Fig. 4d, the adsorption energy of H adatoms is plotted as a function of the chemisorption energy of N adatoms on selected, close packed metal surfaces. The relation is linear between these adsorption energies. In the Discussion section, we use this linear relation to relate the H adsorption energy to the adsorption energy of N adatoms.

4 Discussion

The calculated results presented in the previous section can now be used to estimate two possible variations in the system: (1) the effect of applying an electric potential, and (2) the effect of replacing Ru with some other transition metal. Plotting these two variables constructs so-called volcano plots.

4.1 Applied potential on a Ru electrode

We now use the approach described in Section 2.2 to estimate the effect of an applied bias on the elementary steps in the reduction of nitrogen at a Ru electrode. Assuming an electrolyte solution with pH = 0, room temperature and 1 bar pressure of H_2 gas, the results for the gas phase reduction at steps can be directly related to the electrochemical reduction steps.[30] The only difference is the change in the free energy of the electrons in the electrode when the electric potential is applied, as given in eqn (23). By applying an electric potential which raises the free energy of the electrons in the metal electrode and hence drives protons from the electrolyte towards the metal surface, the uphill reaction steps can be eliminated. We will assume that the onset of a significant reaction rate occurs at a potential where the initial and final states of an elementary step have the same free energy, $\Delta G = 0$. This approach has been successfully applied to other electrochemical reactions.[30,38,39,53]

First, we focus on the associative mechanism, which is analogous to the mechanism in the enzyme. The free energy variation in the presence of an applied bias is shown in Fig. 1 for the flat Ru(0001) surface. When hydrogen is added in the form of H_2 molecules, the reaction has significant thermochemical free energy barriers, as has

been noted previously.[13] In the enzyme, however, hydrogen is not entering as H_2 but as protons and electrons, H^+ and e^-. The free energy variation changes significantly when the chemical potential of the protons and the electrons is increased by applying a negative electric potential. With a potential of $U = -1.08$ V $vs.$ SHE, the free energy rise upon adding the first proton to N_2 is eliminated and all steps become downhill in free energy (exergonic). It is noted here that at this stage we have not yet considered the competing reaction, H_2 formation. For this negative potential and on a Ru electrode, hydrogen gas will be formed in much higher quantities than ammonia.

A much smaller potential is needed if the N_2 is bound to a step site. There, a potential of $U = -0.43$ V or $U = -0.94$ V suffices to make the reaction downhill in free energy at each step, as shown in Fig. 2a and b, for mechanisms a and b, respectively.

In the dissociative mechanism, see Fig. 3, it is enough to apply a potential of -0.16 V to eliminate the reaction free energy of the most difficult step. After the dissociation of the N_2 molecule, all steps in the formation of adsorbed ammonia molecules are then downhill in free energy. The next step would be to further protonate the adsorbed NH_3 to form NH_4^+ solvated in the electrolyte. The last step is not shown in the figure since that requires more detailed modeling of the solvated NH_4^+ ion in the liquid and will be the subject of future work.

4.2 Volcano plots for ammonia formation

The question now arises whether other transition metal surfaces than Ru can be better catalysts for the electro-chemical reaction. By using the linear relations for NH_x and N_2H_x adsorption as a function of the binding energy of N adatoms presented in Fig. 4, one can create volcano plots to see which value of the binding energy of N adatoms would provide the lowest onset potential for electrochemical ammonia synthesis. This method was introduced in ref. 38 where it was applied to the electrolysis of water on oxide surfaces.

In this analysis, the reaction free energy can be used directly as a simple measure of electro-catalytic activity. The reaction free energy for each elementary step can be expressed as a function of the applied bias U and the binding energy of the nitrogen adatom, denoted as N*, in the following way. First, we consider a Heyrovsky-type reaction with an associative mechanism, where solvated protons from the solution can directly react with an electron and N_2H_x or NH_x species on the surface:

$$N_{2(g)} + 6(H^+ + e^-) \rightarrow *N_2H + 5(H^+ + e^-),$$

$$\Delta G_{1,Y-Fe} = \Delta G_{*N_2H} - \Delta G_{N_{2(g)}}$$

$$= \Delta E_{*N_2H} + 0.80 \text{ eV} - 0 \text{ eV} + eU$$

$$= 1.61\Delta E_{*N} + 2.22 \text{ eV} + eU \tag{24}$$

$$N_{2(g)} + 6(H^+ + e^-) \rightarrow *N_2H + 5(H^+ + e^-),$$

$$\Delta G_{1,Fe-Ag} = \Delta G_{*N_2H} - \Delta G_{N_{2(g)}}$$

$$= \Delta E_{*N_2H} + 0.80 \text{ eV} - 0 \text{ eV} + eU \tag{25}$$

$$= 0.59\Delta E_{*N} + 1.31 \text{ eV} + eU$$

$$*N_2H + 5(H^+ + e^-) \rightarrow *NNH_2 + 4(H^+ + e^-),$$

$$\Delta G_{2,Y-Os} = \Delta G_{*NNH_2} - \Delta G_{*N_2H}$$

$$= \Delta E_{*NNH_2} + 1.11 \text{ eV} \tag{26}$$

$$- \Delta E_{*N_2H} - 0.8 \text{ eV} + eU$$

$$= -0.56\Delta E_{*N} - 0.50 \text{ eV} + eU$$

$$*N_2H + 5(H^+ + e^-) \rightarrow *NNH_2 + 4(H^+ + e^-),$$

$$\Delta G_{2,Os-Ag} = \Delta G_{*NNH_2} - \Delta G_{*N_2H}$$

$$= \Delta E_{*NNH_2} + 1.11 \text{ eV} \tag{27}$$

$$- \Delta E_{*N_2H} - 0.8 \text{ eV} + eU$$

$$= +0.05\Delta E_{*N} - 0.01 \text{ eV} + eU$$

$$*NNH_2 + 4(H^+ + e^-) \rightarrow *N + NH_3 + 3(H^+ + e^-),$$

$$\Delta G_{3,Y-Os} = \Delta G_{*N} + \Delta G_{NH_{3(g)}} - \Delta G_{*NNH_2}$$

$$= \Delta E_{*N} + 0.26 \text{ eV} - 0.31 \text{ eV} \tag{28}$$

$$- \Delta E_{*NNH_2} - 1.11 \text{ eV} + eU$$

$$= -0.05\Delta E_{*N} - 1.77 \text{ eV} + eU$$

$$*NNH_2 + 4(H^+ + e^-) \rightarrow *N + NH_3 + 3(H^+ + e^-),$$

$$\Delta G_{3,Os-Ag} = \Delta G_{*N} + \Delta G_{NH_{3(g)}} - \Delta G_{*NNH_2}$$

$$= \Delta E_{*N} + 0.26 \text{ eV} - 0.31 \text{ eV} \tag{29}$$

$$- \Delta E_{*NNH_2} - 1.11 \text{ eV} + eU$$

$$= 0.36\Delta E_{*N} - 1.35 \text{ eV} + eU$$

$$*N + 3(H^+ + e^-) \rightarrow *NH + 2(H^+ + e^-),$$

$$\Delta G_4 = \Delta G_{*NH} - \Delta G_{*N}$$

$$= \Delta E_{*NH} + 0.57 \text{ eV} \tag{30}$$

$$- \Delta E_{*N} - 0.26 \text{ eV} + eU$$

$$= -0.24\Delta E_{*N} - 0.41 \text{ eV} + eU$$

$$*NH + 2(H^+ + e^-) \rightarrow *NH_2 + (H^+ + e^-),$$

$$\Delta G_5 = \Delta G_{*NH_2} - \Delta G_{*NH}$$

$$= \Delta E_{*NH_2} + 0.88 \text{ eV} \tag{31}$$

$$- \Delta E_{*NH} - 0.57 \text{ eV} + eU$$

$$= -0.33\Delta E_{*N} + 0.15 \text{ eV} + eU$$

$$*NH_2 + (H^+ + e^-) \rightarrow NH_{3(g)},$$

$$\Delta G_6 = \Delta G_{NH_{3(g)}} - \Delta G_{*NH_2}$$

$$= -0.31 \text{ eV} - \Delta E_{*NH_2} - 0.88 \text{ eV} + eU$$

$$= -0.43\Delta E_{*N} - 0.31 \text{ eV} + eU$$

$$\tag{32}$$
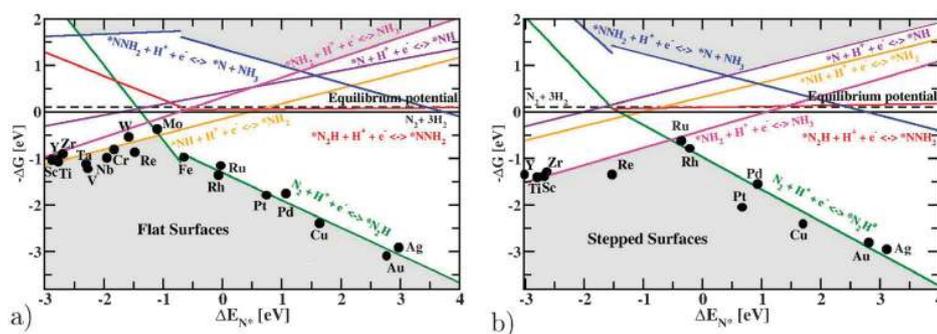
Fig. 5 Negative of the change of the free energy, $-\Delta G$, which within our approximations is proportional to the onset potential, for all the charge transfer steps of ammonia synthesis as a function of the nitrogen binding energy at $U = 0$ V *vs.* SHE. ΔG is calculated from linear relations (lines) as explained in the text. The data points are the DFT values of $-\Delta G$ for the reaction step determining the onset potential. The resulting volcanos are indicated with the shaded areas. The best possible material would fall on the horizontal dashed line representing the theoretical equilibrium potential $+0.1$ V. (a) is for flat surfaces and (b) for stepped surfaces *via* the Heyrovsky-type associative mechanism.

The free energy is expressed here as a sum of an energy contribution that scales as the adatom binding energy, a constant coming from zero point energy and entropy, and the energy shift due to the applied potential. The energy of all the different N_2H_x and NH_x species is now expressed in terms of the N adatom binding energy by using the linear scaling relations from Fig. 4. The energy relations and the constants in eqn (24)–(32) are shown for flat surfaces, whereas similar equations may be written for stepped surfaces.

The negative of the change of the free energy, $-\Delta G$, which within our approximations gives the onset potential, is shown in Fig. 5a and b for the six charge transfer reaction steps of the Heyrovsky-type reaction, eqn (24)–(32). A volcano plot is obtained in both cases, where the right side of the volcano is limited by the first proton transfer step (and adsorbing $N_{2(g)}$), eqn (24), (green lines) both for the flat and the stepped surface. The left side of the volcano is limited by the fifth proton transfer step, eqn (31) (yellow line) for the flat surfaces whereas the last proton transfer step, eqn (32), (magenta line) is the limiting step for the stepped surfaces.

The predicted onset potential for ammonia formation is slightly smaller for the flat surfaces than the stepped surfaces for the left side of the volcano. The stepped surfaces are, however, more catalytically active than the flat surfaces for the right side of the volcano. The top of the volcano is shifted to the right, from approximately -1 eV for the flat surfaces to -0.5 eV for the stepped surfaces. Mo is closest to the top for the flat surfaces, and is, therefore, the best catalyst among the metals considered here.

The estimated electrical potential needed to form ammonia is about -0.5 V for the flat Mo surface. It should be noted here that by turning Fig. 5 upside down the same analysis may be applied to the reverse reaction: ammonia decomposition (oxidation) into nitrogen gas, protons and electrons.

The main reason why the steps are more active than the flat surfaces on the right side of the volcano is because of the stable configuration possible for N_2H at a step, as shown in configuration a in Fig. 2c, which is not possible on a flat surface. This makes the first hydrogenation at a step less endothermic than on the flat surface.

At a negative applied bias most surfaces will be fully covered with H adatoms[36] which will make the N_2H configuration less likely to form. A H adatom needs to be turned into a solvated proton and an electron (Volmer oxidation reaction: $*H \rightarrow H^+ + e^- + *$) to free up a site on the lower terrace. We have, therefore, also considered configuration b in Fig. 2c which does not need two empty sites. The trends and linear relations for configuration b are quite similar to that for configuration a, *cf.* Fig. 4c.

Next, we consider the dissociative mechanism:

$$N_{2(g)} \rightarrow *2N,$$

$$\begin{aligned} \Delta G_1 &= 2\Delta G_{*N} - \Delta G_{N_{2(g)}} \\ &= 2(\Delta E_{*N} + 0.26 \text{ eV}) - 0 \text{ eV} \\ &= 2\Delta E_{*N} + 0.52 \text{ eV} \end{aligned} \qquad (33)$$
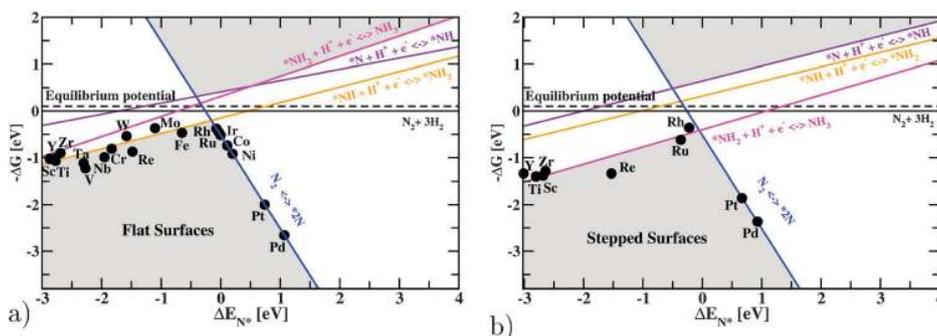
Fig. 6 Similar to Fig. 5, but here for the dissociative mechanisms.

1242 | *Phys. Chem. Chem. Phys.*, 2012, **14**, 1235–1245

This journal is © the Owner Societies 2012

and the remaining equations are the same as eqn (30)–(32). In both cases the N_2 splitting is the most difficult step at the right leg of the volcanos in Fig. 6. For the more active volcano, Fig. 6a, the left leg is limited by the protonation of the NH species on the flat surface. This is the same step as for the associative mechanism on the flat surfaces. The estimated electric potential needed to form ammonia is about -0.35 V for the optimal flat surface *via* the dissociative mechanism.

N_2 dissociation is very slow on flat surfaces of Fe and Ru and it has been shown that defects are necessary to split the strong triple bond of N_2.[51] To get a reasonable rate the temperature is increased to approximately 700 K.[6,8] Hence, these metals (and more noble metals) will not be able to split the N_2 bond with a reasonable rate at room temperature. However, since the early transition metals bind atomic nitrogen strongly the reaction will be very exothermic with a small or no activation barrier, even on the flat terraces. The dissociative mechanism is thus possible on the early transition metals at room temperature, whereas it is impossible on the late transition metals. From Fig. 6 we see for the early transition metals that the flat surfaces have lower over-potential than their stepped counterparts.

Fig. 7 shows a combined volcano diagram from the four volcanoes displayed in Fig. 5 and 6; the dissociative (solid lines) and associative (dashed lines) mechanisms on both flat (black) and stepped (red) surfaces. The H-bonds effect has been included (dotted lines) as described above in Section 2.2. Considering the metals on the right legs of the volcanoes to start with, for both of the surface structures the adsorption of molecular nitrogen and the first proton transfer step ($N_{2(g)} + H^+ + e^- \rightarrow *N_2H$) is determining the onset potential for the associative mechanism, whereas the N_2 splitting is determining the rate for the dissociative mechanism. The metals on the left legs have the same reaction steps determining the onset potential for the dissociative and the associative mechanism; the $*NH + H^+ + e^- \rightarrow *NH_2$ reaction on the flat surfaces and the $*NH_2 + H^+ + e^- \rightarrow NH_{3(g)}$ reaction on the stepped surfaces.

The main problem is that the formation of hydrogen gas can end up being very fast unless the surface is covered with N-adatoms rather than H-adatoms. A calculated phase diagram showing whether the surface is covered with adsorbed N-atoms or H-atoms is also shown in Fig. 7. The reference state is N_2 and H_2 in the gas phase at 1 bar. The free energy of N- and H-adatoms is taken to be a function of the same descriptor as used in the volcanos, the nitrogen binding energy, by using the linear relation of *H *vs.* *N adsorption energy from Fig. 4d. From this analysis, only the flat metal surfaces of Sc, Y, Ti and Zr are expected to be covered with N instead of H, at the negative bias needed for the ammonia synthesis to be downhill at these particular metals. Combining this result with the free energy difference of *NH *vs.* *H (vertical line a in Fig. 7) and of $*NH_2$ *vs.* H_2 (line b), we predict flat metal surfaces of Sc, Y, Ti and Zr to form ammonia with the dissociative mechanism rather than H_2 molecules.

The free energy difference of $*N_2H$ *vs.* *H (line c) and of $*N_2H_2$ *vs.* H_2 (line d) indicates on which metal surfaces the species needed for the associative mechanism for ammonia formation are lower in free energy than the species needed to
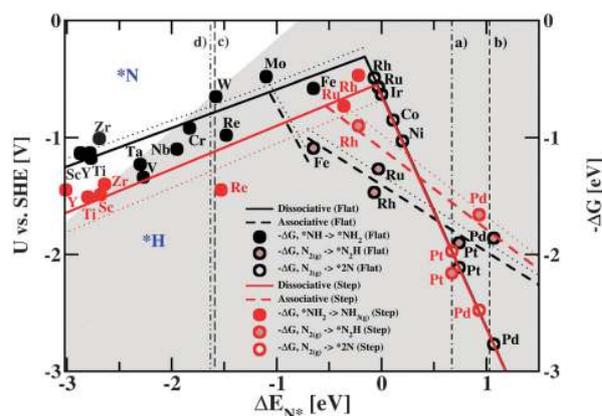
Fig. 7 Combined volcano diagrams (lines) for the flat (black) and stepped (red) transition metal surfaces for reduction of nitrogen with a Heyrovsky type reaction, without (solid lines) and with (dotted lines) H-bonds effect. The data points are the DFT values of $-\Delta G$ for a given reaction step. The volcano is constructed by combining together the four volcano diagrams in Fig. 5 and 6 for the dissociative (solid lines) and associative (dashed lines) mechanisms on both flat and stepped surfaces. For both surface structures the adsorption of molecular nitrogen and the first proton transfer step ($N_{2(g)} + H^+ + e^- \rightarrow *N_2H$) is determining the activity of the metals on the right legs of the volcanoes for the associative mechanism whereas the N_2 splitting is rate determining for the dissociative mechanism. The metals on the left legs have the same rate-determining steps for the dissociative and the associative mechanisms; the $*NH + H^+ + e^- \rightarrow *NH_2$ reaction on the flat surfaces and the $*NH_2 + H^+ + e^- \rightarrow NH_{3(g)}$ reaction on the stepped surfaces. The horizontal axis gives the binding energy of N-adatoms, which is used as a descriptor. The grey shaded area indicates the conditions under which the surface will likely be covered with H-adatoms. The white area indicates for which metals and at which bias values the surfaces will be covered with N-adatoms instead of H-adatoms. This is done by comparing the free energy change of $N_2 \rightarrow *2N$ and $H_2 \rightarrow 2(H^+ + e^-) \rightarrow *2H$. The vertical lines (a, b, c, and d) indicate which species are most strongly bound to the surface when comparing reactions involving the same number of protons/electrons. To the left of the line labeled a, *NH is lower in free energy than *H adsorbed on the surface and N_2 in the gas phase. To the left of line b, $*NH_2$ is lower in free energy than N_2 and H_2 in the gas phase. To the left of line c is where $*N_2H$ species have lower free energy on the surface than *H species on the surface and N_2 in the gas phase. To the left of line d is where $*N_2H_2$ species have lower free energy than N_2 in the gas phase and if the two protons and electrons are used to form H_2 instead of reducing N_2.

form H_2 molecules. According to this analysis, the $*N_2H_x$ species are more stable than *H or $H_{2(g)}$ on Cr and more reactive metals. However, N_2 dissociation will occur quite readily on these surfaces anyway and the dissociative mechanism will thus be more likely than the associative mechanism for the early transition metals but the analysis has not taken lateral interactions into account nor possible activation energy barriers of these elementary steps.

This overall picture shows that the flat transition metal surfaces of Sc, Y, Ti, and Zr should be able to reduce N_2 to NH_3 (without making too much H_2 at the same time) *via* the dissociative mechanisms if a bias of *ca.* -1 V to -1.5 V *vs.* NHE is used. The analysis presented above and shown in Fig. 7 can explain why the kinetics of N_2 reduction in the

experimental studies carried out so far[21–28] have been too slow in comparison to H_2 production. The Ru and Pt electrodes which were usually used would have been covered with hydrogen at negative bias and nitrogen would not have been able to adsorb and get reduced to ammonia. By using some of the early transition metals such as Sc, Y, Ti, or Zr, N-adatoms would bind more strongly on the electrode surface than H-adatoms and should get reduced to form $NH_{3(g)}$ more readily than forming $H_{2(g)}$, even at quite negative potentials.

5 Conclusions

Our theoretical analysis of the possibility of forming ammonia electrochemically on pure transition metal electrodes indicates that a dissociative mechanism, analogous to the Haber–Bosch industrial process, could yield ammonia, especially on flat surfaces of the early transition metals Sc, Y, Ti, and Zr and negative potential bias at around -1.0 V to -1.5 V with respect to SHE. Hydrogen gas formation will be a competing reaction for all other transition metal surfaces as it is for nitrogenase. But, since protons in the electrolyte most likely add directly to an adsorbed nitrogen (Heyrovsky type reaction) and some of the promising metal surfaces such as Sc, Y, Ti, and Zr bind N-adatoms more strongly than H-adatoms, a significant amount of ammonia compared with hydrogen gas can be expected.

The effect of an applied bias and the trends over a range of transition metal electrodes have been established using DFT calculations and harmonic approximation to estimate free energy of adsorbed species. Several other significant approximations are also invoked: (1) lateral interactions in the adsorbates are neglected and (2) the possibility of potential-dependent/independent activation barriers that are larger than those dictated by the thermodynamics have not been included. (3) We have not included a water phase explicitly in the DFT calculations, but we estimate the effect of H-bonds with water in an approximated way. A more detailed study should include these calculations and this will be the subject of future work. Despite the approximations we have made, we believe that the qualitative conclusions drawn are valid and the results presented here will hopefully encourage experimentalists to study the N_2 reduction into ammonia on some of the early transition metals.

References

1 V. Smil, *Sci. Am.*, 1997, **277**, 76.
2 G. Ertl, *J. Vac. Sci. Technol., A*, 1983, **1**, 1247.
3 G. Ertl, *Angew. Chem., Int. Ed.*, 2008, **47**, 3524.
4 N. D. Spencer, R. C. Schoonmaker and G. A. Somorjai, *J. Catal.*, 1982, **74**, 129.
5 P. Stoltze and J. K. Nørskov, *Phys. Rev. Lett.*, 1985, **55**, 2502.
6 S. R. Tennison, in *Catalytic Ammonia Synthesis Fundamentals and Practice*, ed. J. Jennings, Plenum Press, New York, 1991, vol. 303.
7 H. Topsøe, M. Boudart and J. K. Nørskov, *Frontiers in Catalysis*, in *Topics in Catalysis*, Baltzer, Basel, 1994, vol. 1.
8 K. Aika and H. Tamura, *Ammonia: Catalysis and Manufacture*, in *Ammonia synthesis over non-iron catalysts and related phenomena*, ed. A. Nielsen, Springer, Berlin, 1995, vol. 103, pp. 103–148.
9 R. Schlögl, *Angew. Chem., Int. Ed.*, 2003, **42**, 2004.
10 K. Honkala, A. Hellman, I. N. Remediakis, A. Logadóttir, A. Carlsson, S. Dahl, C. H. Christensen and J. K. Nørskov, *Science*, 2005, **307**, 555.
11 L. Stryer, *Biochemistry*, W.H. Freeman, New York, 4th edn, 1995.
12 B. K. Burgess and D. J. Lowe, *Chem. Rev.*, 1996, **96**, 2983.
13 T. H. Rod, A. Logadóttir and J. K. Nørskov, *J. Chem. Phys.*, 2000, **112**, 5343.
14 A. Hellman, M. Biczysko, T. Bligaard, C. H. Christensen, D. C. Clary, S. Dahl, R. van Harrevelt, K. Honkala, H. Jónsson, M. Luppi, E. J. Baerends, G. J. Kroes, U. Manthe, J. K. Nørskov, R. A. Olsen, J. Rossmeisl, E. Skúlason, C. S. Tautermann, A. J. C. Varandas and J. K. Vincent, *J. Phys. Chem. B*, 2006, **110**, 17719.
15 I. Dance, *Chem. Commun.*, 1997, 165.
16 T. H. Rod, B. Hammer and J. K. Nørskov, *Phys. Rev. Lett.*, 1999, **82**, 4054.
17 T. H. Rod and J. K. Nørskov, *J. Am. Chem. Soc.*, 2000, **122**, 12751.
18 B. M. Hoffman, D. R. Dean and L. C. Seefeldt, *Acc. Chem. Res.*, 2009, **42**, 609.
19 D. V. Yandulov and R. R. Schrock, *Science*, 2003, **301**, 76.
20 F. Studt and F. Tuczek, *Angew. Chem., Int. Ed.*, 2005, **44**, 5639.
21 G. Marnellos and M. Stoukides, *Science*, 1998, **282**, 98.
22 V. Kordali, G. Kyriacou and C. Lambrou, *Chem. Commun.*, 2000, 1673.
23 G. Marnellos, S. Zisekas and M. Stoukides, *J. Catal.*, 2000, **193**, 80.
24 T. Murakami, T. Nishikiori, T. Nohira and Y. Ito, *J. Am. Chem. Soc.*, 2003, **125**, 334.
25 A. Denvir, O. Murphy, A. Cisar, P. Robertson and K. Uselton, *US Patent*, 6,881,208 B2, 2005.
26 T. Murakami, T. Nohira, T. Goto, Y. Ogata and Y. Ito, *Electrochim. Acta*, 2005, **50**, 5423.
27 T. Murakami, T. Nohira, Y. Araki, T. Goto, R. Hagiwara and Y. Ogata, *Electrochem. Solid-State Lett.*, 2007, **10**, E4.
28 M. Ouzounidou, A. Skodra, C. Kokkofitis and M. Stoukides, *Solid State Ionics*, 2007, **178**, 153.
29 A. Logadóttir, T. Rod, J. K. Nørskov, B. Hammer, S. Dahl and C. J. H. Jacobsen, *J. Catal.*, 2001, **197**, 229.
30 J. K. Nørskov, J. Rossmeisl, A. Logadóttir, L. Lindqvist, J. R. Kitchin, T. Bligaard and H. Jónsson, *J. Phys. Chem.*, 2004, **108**, 17886.
31 *Dacapo pseudopotential code*. URL http://www.fysik.dtu.dk/campos. (Center for Atomic-scale Materials Design, Technical University of Denmark, 2011).
32 B. Hammer, L. B. Hansen and J. K. Nørskov, *Phys. Rev. B: Condens. Matter*, 1999, **46**, 7413.
33 J. Tafel, *Z. Phys. Chem., Stoechiom. Verwandtschaftsl.*, 1905, **50**, 641.
34 J. Heyrovsky, *Recl. Trav. Chim. Pays-Bas*, 1927, **46**, 582.
35 E. Skúlason, G. Karlberg, J. Rossmeisl, T. Bligaard, J. Greeley, H. Jónsson and J. K. Nørskov, *Phys. Chem. Chem. Phys.*, 2007, **9**, 3241.
36 E. Skúlason, V. Tripkovic, M. Björketun, S. Gudmundsdóttir, G. Karlberg, J. Rossmeisl, T. Bligaard, H. Jónsson and J. Nørskov, *J. Phys. Chem. C*, 2010, **114**, 18182.
37 S. Wang, V. Petzold, V. Tripkovic, J. Kleis, J. G. Howalt, E. Skúlason, E. M. Fernández, B. Hvolbaek, G. Jones, A. Toftelund, H. Falsig, M. Björketun, F. Studt, F. Abild-Pedersen, J. Rossmeisl, J. K. Nørskov and T. Bligaard, *Phys. Chem. Chem. Phys.*, 2011, **13**, 20760.
38 J. Rossmeisl, Z.-W. Qu, H. Zhu, G.-J. Kroes and J. K. Nørskov, *J. Electroanal. Chem.*, 2007, **607**, 83.
39 A. A. Peterson, F. Abild-Pedersen, F. Studt, J. Rossmeisl and J. K. Nørskov, *Energy Environ. Sci.*, 2010, **3**, 1311.
40 P. W. Atkins, *Physical Chemistry*, Oxford University Press, Oxford, 6th edn, 1998, pp. 485, 866–867, 925–927 and 942.

41 A. Roudgar and A. Groß, *Chem. Phys. Lett.*, 2005, **409**, 157.
42 J. Rossmeisl, J. K. Nørskov, C. Taylor, M. Janik and M. Neurock, *J. Phys. Chem. B*, 2006, **110**, 21833.
43 G. S. Karlberg, J. Rossmeisl and J. K. Nørskov, *Phys. Chem. Chem. Phys.*, 2007, **9**, 5158.
44 G. S. Karlberg and G. Wahnström, *Phys. Rev. Lett.*, 2004, **92**, 136103.
45 J. Rossmeisl, J. Greeley and G. S. Karlberg, in *Fuel Cell Catalysis: A Surface Science Approach*, ed. M. T. M. Koper, John Wiley & Sons, Inc., Hoboken, NJ, USA, 2009, p. 57.
46 V. Tripkovic, E. Skúlason, S. Siahrostami, J. K. Nørskov and J. Rossmeisl, *Electrochim. Acta*, 2010, **55**, 7975.
47 J. W. Larson and T. B. McMahon, *Inorg. Chem.*, 1984, **23**, 2029.

48 T. R. Mattsson and S. J. Paddison, *Surf. Sci.*, 2003, **544**, L697.
49 F. Abild-Pedersen, J. Greeley, F. Studt, J. Rossmeisl, T. Munter, P. Moses, E. Skúlason, T. Bligaard and J. K. Nørskov, *Phys. Rev. Lett.*, 2007, **99**, 016105.
50 G. Jones, F. Studt, F. Abild-Pedersen, J. K. Nørskov and T. Bligaard, *Chem. Eng. Sci.*, 2011, **66**, 6318.
51 S. Dahl, A. Logadottir, R. C. Egeberg, J. H. Larsen, I. Chorkendorff, E. Törnqvist and J. K. Nørskov, *Phys. Rev. Lett.*, 1999, **83**, 1814.
52 A. Logadóttir and J. K. Nørskov, *J. Catal.*, 2003, **220**, 273.
53 H. A. Hansen, I. C. Man, F. Studt, F. Abild-Pedersen, T. Bligaard and J. Rossmeisl, *Phys. Chem. Chem. Phys.*, 2010, **12**, 283.